Energies **2015**, *8*, 837-858; doi:10.3390/en8020837

OPEN ACCESS

energies

ISSN 1996-1073

www.mdpi.com/journal/energies

Article

Contamination Grades Recognition of Ceramic Insulators Using Fused Features of Infrared and Ultraviolet Images

Lijun Jin [1,2,*] and Da Zhang [1]

[1] School of Electronics and Information Engineering, Tongji University, Shanghai 201804, China; E-Mail: qdzd721@163.com

[2] State Key Laboratory of Electrical Insulation and Power Equipment, Xi'an Jiaotong University, Xi'an 710049, China

***** Author to whom correspondence should be addressed; E-Mail: jinlj@mail.tongji.edu.cn; Tel.: +86-21-6958-9378; Fax: +86-21-6958-9241.

Academic Editor: Chang Sik Lee

Received: 1 December 2014 / Accepted: 9 January 2015 / Published: 27 January 2015

Abstract: In order to realize the non-contact measurement of ceramic insulator contamination severity, a method based on feature level fusion of infrared (IR) and ultraviolet (UV) image information is proposed in this paper. IR and UV images of artificially polluted insulators were obtained from high voltage experiments at 80%, 85% and 90% RH. After the preprocessing of images, IR and UV features were calculated, respectively. Then, feature selection based on Fisher criterion was adopted to gain features, which have the ability to distinguish different contamination grades effectively. In feature level fusion section, kernel principal component analysis (KPCA) was applied to the dimensionality reduction fusion of IR and UV features and obtain three-dimensional fused features. A particle swarm optimized back propagation neural network (PSO-BPNN) classifier was constructed and trained to recognize the contamination grades. Experimental results indicate that the feature level fusion of IR and UV information based on KPCA has capability to characterize the contamination grades comprehensively. Compared with recognition using IR or UV features separately, recognition based on the feature level fusion is more accurate and effective. This study provides a new methodology for the measurement of insulator contamination severity at working condition.

Keywords: contamination grades; infrared images; ultraviolet images; feature level fusion; Fisher criterion; kernel principal component analysis; particle swarm optimization

1. Introduction

With the expansion of power grid and the increase of voltage class, insulator contamination flashover has been a direct threat to the safety of power systems. Under the operating voltage, contaminants in combination with moisture cause the reduction of surface insulation strength and the flow of leakage currents. The appearance of dry bands on the insulator surface causes electrical discharges and arcs. At high humidity, such arcs may elongate and cause flashover [1–4]. According to International Electrotechnical Commission Standard (IEC 60507), the severity of contamination is divided into four grades (I, II, III, IV). From grade I to grade IV, the contamination severity changes from mild to serious. At present, the most effective way to prevent the contamination flashover is cleaning the contaminated insulators in forms of hot washing or hand sweeping. This paper comes from a cooperation project with China Southern Power Grid Company Limited (CSG). The ultimate goal of our research is to provide a Condition Based Maintenance (CBM) technique for the prevention of contamination flashover. As the rapid development of industries and urbanization in China, environmental pollution (including industrial pollution, automobile exhaust and raise dust) is increasingly serious. And the pattern of pollution accumulation in a certain area is often not stable but varying. Therefore, engineers of CSG demand a CBM technique to measure the contamination grades of insulators (insulators near factories or other pollution source or other regions that need attention) in inspection and provide direction for cleaning schedule.

Under the effect of operating voltage, there exist leakage currents on the surface of polluted insulator. As a result of the heating effect of leakage currents, surface temperature of insulator increases. Infrared (IR) images, which have the ability to characterize the temperature distribution on the surface of insulator, can be obtained by infrared thermography [5–7]. Heating power of wet polluted insulator with discharges can be expressed as:

$$P_s = \frac{U_f^2}{R_d + R_p} \tag{1}$$

where U_f is the operating voltage, R_d is the equivalent discharges resistance, R_p is the surface resistance of polluted layer. As insulators with different contamination severities have different surface resistivities, surface temperatures of insulators with different contamination grades are different. Meanwhile, electrical discharges occur on the surface of polluted insulator. Due to the difference in electroconductibility, discharge intensities of insulators with different contamination grades are different. Ultraviolet (UV) imager has the ability to detect the solar blind ultraviolet ray emitted by discharge with wavelength of 240~280 nm and record the discharge phenomenon in forms of image or video. Discharge intensities on the surface of insulators can be evaluated by ultraviolet image or video [8,9]. Compared with other pollution measurement methods, such as equivalent salt deposit density (ESDD) test, leakage current (LC) monitoring [10–16], acoustic emission signal monitoring [17,18], contamination grades recognition using IR or UV image has the following advantages: (1) Non-contact

and non-destructive; (2) No power cut and insurance of the personnel security; (3) Indication of temperature changes; (4) Reflection of discharge intensity. Miniaturized IR and UV imagers can be installed in multiple platforms, such as inspection robot, inspection vehicle, and unmanned aerial vehicle (UAV). As is shown in Figure 1, an inspection robot equipped with IR and UV imagers has the ability to inspect temperature and discharge of insulators in transmission line.

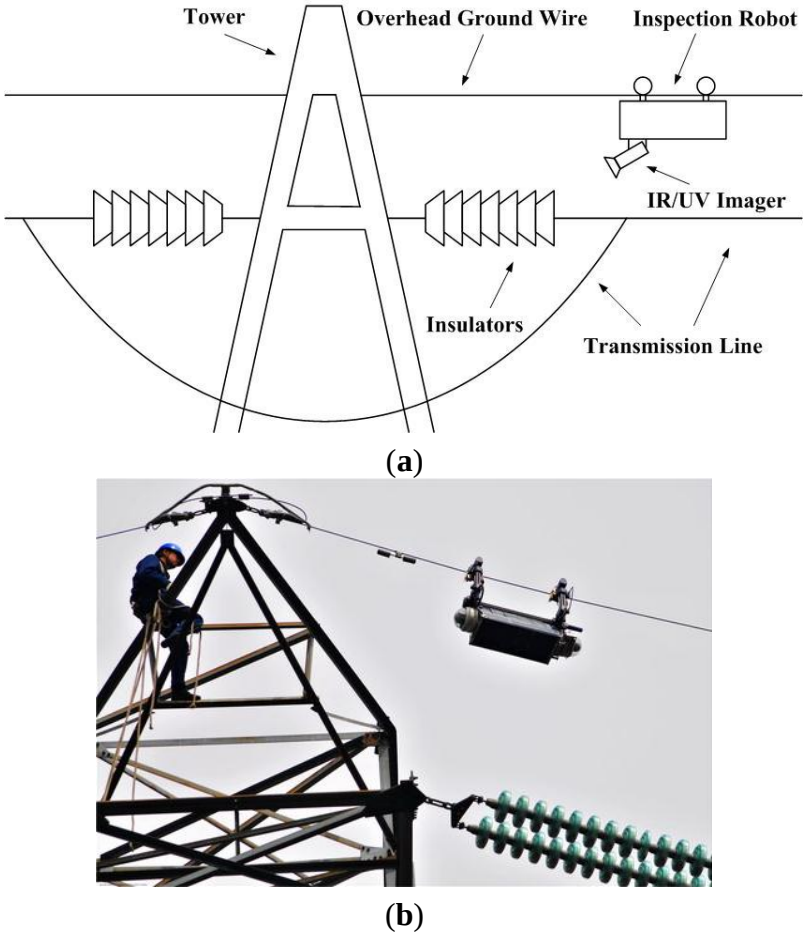

Figure 1. Inspection robot equipped with infrared (IR) and ultraviolet (UV) imagers. (**a**) Schematic illustration of inspection robot used in power line; (**b**) Practical application of inspection robot.

IR and UV images, respectively, describe the characteristics of temperature distribution and discharge intensity of polluted insulators with different contamination grades. Information fusion has the ability to utilize information of two kinds of images comprehensively and improve the precision of contamination grades recognition [19]. Information fusion is the process of combining and integrating features originated from different sources to provide more comprehensive, unified and specific information to a pattern identification problem [20]. Depending on which level the fusion is being done, information fusion methodologies can be divided into two categories. In feature level fusion, the features of different information sources are calculated, respectively, and then fused into a single set utilized by a subsequent classifier. In decision level fusion, data from different sources are processed and classified separately, and then the results are combined in the final fusion step. Compared with decision level fusion, feature level fusion retains more original information and is more reliable in application [21,22]. This paper puts

forward a contamination grades recognition method for ceramic insulator based on the feature level fusion of IR and UV image information. The proposed approach involves five main steps: image capture, preprocessing, feature selection, feature fusion and identification. In image capture step, artificial contamination experiments are carried out in high voltage laboratory and large numbers of IR and UV images are obtained. In preprocessing step, a mathematical morphology improved Otsu algorithm is applied to the image segmentation of IR images and a calculation method of electric discharge spot area of UV images is proposed. Initial features of IR and UV images are calculated after the preprocessing of two kinds of images. In feature selection step, Fisher criterion is adopted to select features, which have the ability to represent the contamination grades efficiently. In feature fusion step, Kernel principal component analysis (KPCA) is used to carry out dimensionality reduction fusion of the combination of IR and UV selected features and obtain three-dimensional fused feature vectors. Meanwhile, based on the variations of cumulative contribution ratios, the selection problems of fused feature dimension and kernel function parameter are studied. In identification step, back propagation neural network (BPNN) classifier is utilized to identify the contamination grades. Particle swarm optimization (PSO) algorithm is applied to optimize the training process of BPNN. Flow chart of the methodology is shown in Figure 2.

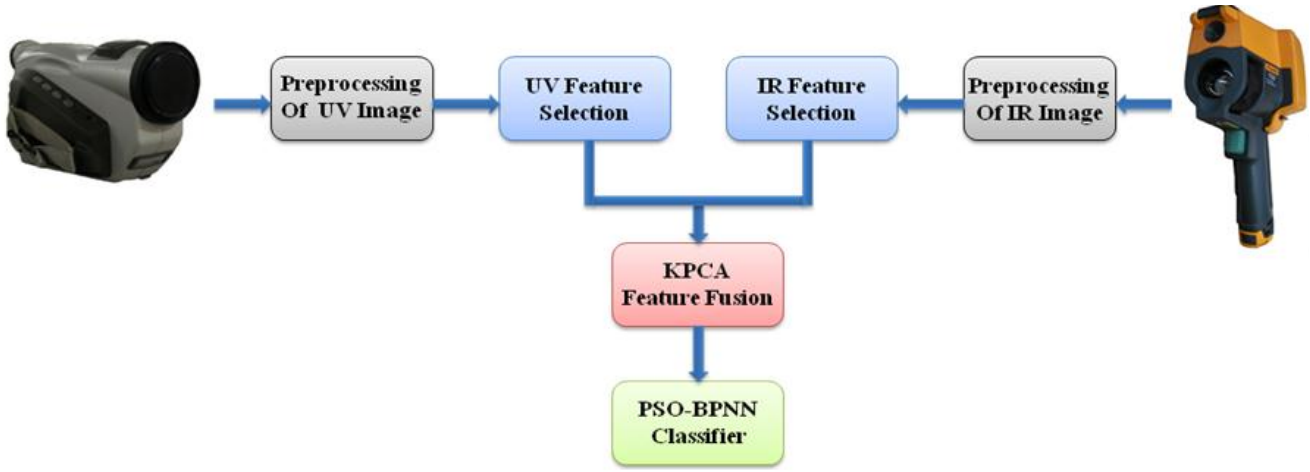

Figure 2. Flow chart of the methodology.

2. Experimental Setup and Procedure

2.1. Design of Experiments

Artificial contamination experiments were carried out in high-voltage laboratory of Shenzhen Power Supply Bureau. In practice, insulators in same string have the similar contamination grades. Recognition result of one insulator can reflect the contamination severity of the whole string. Hence, the study subject can be set as single piece of insulator. Twelve pieces of cap and pin type suspension ceramic insulators of type XP-70 (Dalian Insulator Group Co., Ltd., Dalian, China were used in the experiments. The top surface of XP-70 is 674 cm^2, the bottom surface is 917 cm^2, the creepage distance is 295 cm and the rated voltage is 10 kV. Artificially contaminated insulators are shown in Figure 3.

Figure 3. Artificially contaminated insulators used in experiments.

The test system is shown in Figure 4. Voltmeter and voltage regulator are integrated in a test transformer control box, which controls the operating voltage. Output of the transformer (type GS108, China Electric Equipment Group, Nanjing, China) was connected to the steel nail on the underneath of insulator by a copper wire. And the earth wire was connected to the steel cap. Wires used in experiments were compressed tightly to avoid any discharge caused by poor contact.

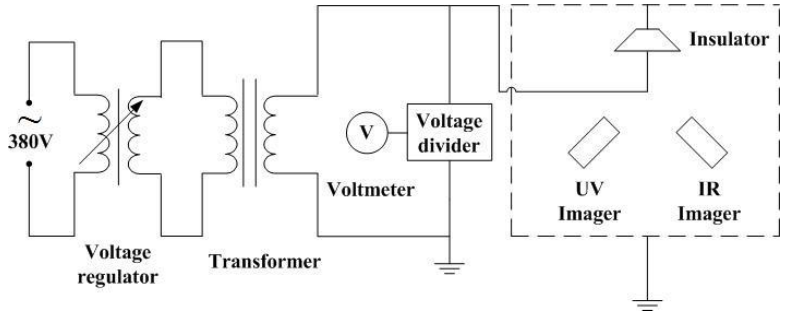

Figure 4. Schematic diagram of the test circuit.

Before the tests, all insulator samples were carefully washed using running water to remove feculence and dried naturally. After the preparation, solid layer method based on IEC 60507 standard was adopted to produce uniform pollution layers on the surface of insulators. The artificial pollutant was made of distilled water, kaolin (substitute for non-soluble substances in natural contaminants) and sodium chloride (NaCl, substitute for soluble salts in natural contaminants). In order to simulate the four contamination grades (I, II, III, IV), insulator samples were divided into four groups. There were three insulators in each group. Values of salt deposit density (SDD) of each group were selected as 0.03–0.06 mg/cm^2 (corresponding to grade I), 0.06–0.1 mg/cm^2 (corresponding to grade II), 0.1–0.25 mg/cm^2 (corresponding to grade III) and 0.25–0.35 mg/cm^2 (corresponding to grade IV). Value of non-soluble deposit density (NSDD) was set as 1 mg/cm^2 for every group. Amounts of sodium chloride and kaolin were calculated by the surface area of insulator, SDD and NSDD. The pollutants were brushed on the surface of insulators uniformly and shady dried for 24 h before the high voltage experiments. In 110 kV transmission line, phase voltage applied to an insulator string with six or seven pieces of insulators is 63.5 kV. In order to simulate the practical situation as far as possible, the test voltage was set as 10 kV, which is the average voltage for a suspension insulator in 110 kV transmission line (10 kV is also the rated voltage of XP-70). When relative humidity (RH) is less than 75%, soluble salt in contaminate does not dissolve obviously and the leakage current value is small. So the temperature rise and discharge on insulator surface are not obvious. In order to simulate insulators at relatively high humidity conditions, the experiments were carried out at relative humidity of 80%, 85% and 90%,

respectively. The permissible variance range of RH was ±2%. Ambient temperature was recorded in synchronization with the shooting of IR image.

2.2. Shooting and Preprocessing of Infrared (IR) Images

According to [6,7], compared with other parts of suspension insulator, temperature rise on the underneath is most obvious and suitable for subsequent analysis and processing. IR images of the underneath of XP-70 suspension insulators were shot at a distance of 2 m by Ti-32 IR imager (Fluke Corporation, Everett, WA, USA). Color palette option of IR imager was set as "Iron Oxide Red". According to [5], it takes about 2 h for a polluted disc suspension insulator to achieve thermal balance. Therefore, IR image shooting was started 2 h later than the beginning of high voltage experiment. Five pieces of IR image of each contamination grade were shot at an interval of 5 min. IR images of insulators with different contamination grades at 85% RH are shown in Figure 5.

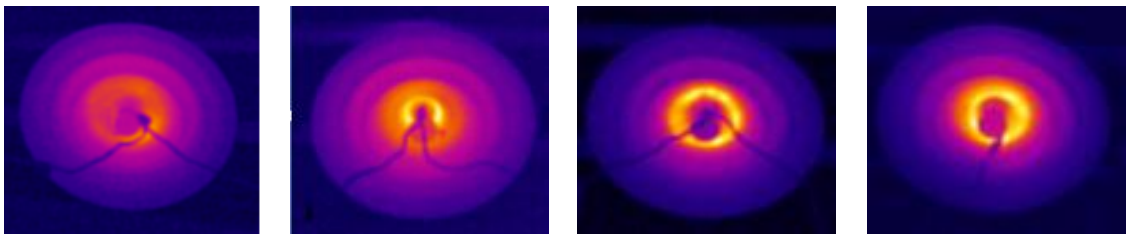

(**a**) (**b**) (**c**) (**d**)

Figure 5. Infrared images of polluted insulators at 85% RH; (**a**) Insulator of I contamination grade; (**b**) Insulator of II contamination grade; (**c**) Insulator of III contamination grade; and (**d**) Insulator of IV contamination grade.

Two files can be obtained from the IR imager. One is IR image in BMP format. The other is temperature data table in Excel format. The size of image and Excel file is 320 × 240. Temperature data of the insulator region is the basis of subsequent analysis. It requires two steps to obtain the temperature data of insulator. The first step is segmenting the insulator from background on IR image and recording the coordinates of insulator region. The second step is reading the corresponding temperature data from Excel file according to the recorded coordinates.

HSI color standard is a common standard for color image display. Hue (H), saturation (S) and intensity (I) are used to display a color image in HSI color space. In order to look for the proper component image for segmentation, HSI component images of IR image are compared in Figure 6.

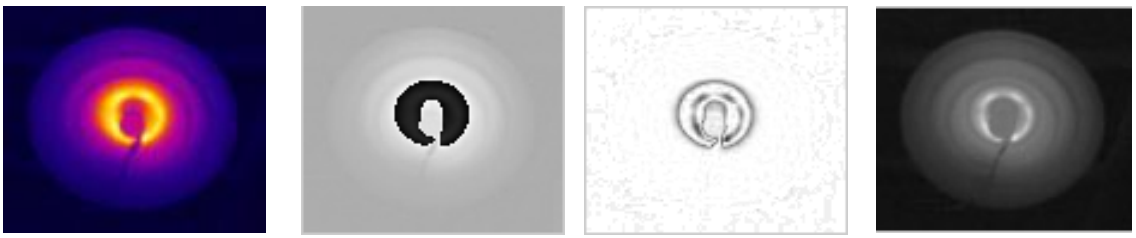

(**a**) (**b**) (**c**) (**d**)

Figure 6. Comparison of images in HSI color space; (**a**) IR image of insulator; (**b**) H component image; (**c**) S component image; and (**d**) I component image.

As is shown in Figure 6, it is hard to distinguish the region of insulator from background in H or S component image. Meanwhile, insulator contour of I component image is relatively clear. Hence I component image was adopted to extract the region of insulator using image segmentation algorithm. In this paper, a mathematical morphology improved Otsu algorithm was proposed to realize the image segmentation. At first, Otsu algorithm was applied to the preliminary segmentation of I component image. After that, further morphological processing was utilized to improve segmentation effect.

Otsu algorithm is a kind of high efficiency image segmentation algorithm, which has the ability to divide object from background without any prior knowledge. Supposing the size of image is $M \times N$, pixel number of the object is N_1, pixel number of the background is N_2. Area proportion of object to entire image is shown in Equation (2):

$$\omega_1 = \frac{N_1}{MN} \tag{2}$$

And area proportion of background to entire image is shown as:

$$\omega_2 = \frac{N_2}{MN} \tag{3}$$

The overall average of gray value is defined in Equation (4):

$$\mu = \mu_1\omega_1 + \mu_2\omega_2 \tag{4}$$

where μ_1 is the average gray value of object and μ_2 is the average gray value of background. Variance of object and background is defined as:

$$g = \omega_1(\mu - \mu_1)^2 + \omega_2(\mu - \mu_2)^2 \tag{5}$$

Traversal method is adopted to obtain the proper segmentation threshold *T*, which ensures that the value of variance g is the maximum of all possible values. Taking IR image of IV contamination grade insulator for example, binary image obtained from Otsu segmentation can be seen in Figure 7b. In binary image, white area represents insulator surface, and black area represents background. As is shown in Figure 7b, the extracted insulator surface is smaller than the actual one and the border is rough. In order to improve the segmentation effect, mathematical morphology methods were used to further process the preliminarily segmented image.

Mathematical morphology is a kind of image analysis methodology based on set theory. Dilation and erosion are two basic operations of mathematical morphology. Different combinations of dilation and erosion constitute various operations such as opening and closing. Size and shape of mathematical morphology is defined by structure element *B*, which is constituted by 0 and 1. An example of square structure element with size of 3 × 3 is shown in Figure 7.

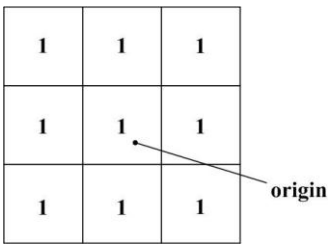

Figure 7. A square structure element with size of 3 × 3.

The dilation operation of image *A* using structure element *B* is defined as:

$$D(A) = A \oplus B = \left\{(x, y)\middle|B_{xy} \cap A \neq \emptyset\right\} \quad (6)$$

When origin of structure element *B* is located in point (*x*, *y*), if intersection of *B* and *A* is a nonempty set, point (*x*, *y*) is a part of dilated binary image *D*(*A*). Dilation leads to the expansion of image. Erosion is the dual operation of dilation. It is defined as follows:

$$E(A) = A\Theta B = \left\{(x, y)\middle|B_{xy} \subseteq A\right\} \quad (7)$$

When origin of structure element *B* is located in point (*x*, *y*), if all points of *B* belong to image *A*, point (*x*, *y*) is a part of eroded binary image *E*(*A*). We can see that erosion leads to the shrinking of the image. Opening and closing are combinations of dilation and erosion. The opening operation of image *A* using structure element *B* is defined as:

$$A \circ B = (A\Theta B)\oplus B \quad (8)$$

The closing operation of image *A* using structure element *B* is defined as:

$$A \bullet B = (A\oplus B)\Theta B \quad (9)$$

Dilation operation leads to the expansion of image outline. Erosion operation leads to the shrinking of the image outline. Opening operation has the ability to break narrow connections and eliminate tiny protrusions. Closing operation has the ability to bridge slender gaps and fill small holes. In our study, a square structure element with size of 10 × 10 was applied to morphological processing. In order to eliminate protrusions, gaps and holes on the surface of insulator, the binary image obtained from Otsu algorithm was processed by opening and closing. After that, the image was dilated to expand the surface area of insulator. As is shown in Figure 8c, morphological processing improves the segmentation effect significantly and the extracted insulator surface is close to the actual one.

(**a**) (**b**) (**c**)

Figure 8. Result of image segmentation; (**a**) IR image of insulator; (**b**) Binary image after Otsu segmentation; and (**c**) Binary image after morphological processing.

Distribution curves of mean temperatures and max temperatures of insulators with different contamination grades at different environment conditions (relative humidity and ambient temperature) are shown in Figure 9. It can be seen that surface temperature of the contaminated insulator rises significantly in humid condition. Temperature rises of insulators with high contamination grades are more obvious than that of insulators with low contamination grades. As the temperature differences between each contamination grade are relatively small, it is difficult to establish a precise mathematical model between contamination grades and temperature characteristics. Therefore, artificial intelligent

methodologies, such as information fusion and pattern recognition are applied to the contamination grades recognition in this study.

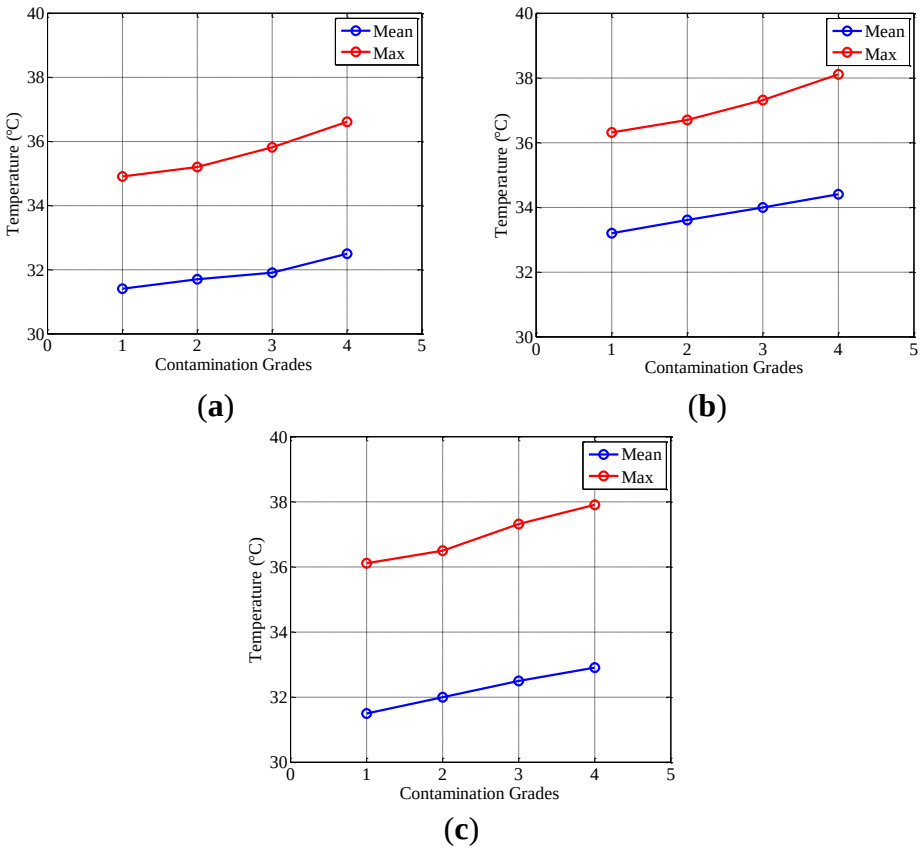

Figure 9. Distribution curves of mean temperature and max temperature. (**a**) RH = 80%, ambient temperature is 29 ℃; (**b**) RH = 85%, ambient temperature is 30.2 ℃; (**c**) RH = 90%, ambient temperature is 28.3 ℃.

2.3. Shooting and Preprocessing of Ultraviolet (UV) Images

As mentioned in [6,7], area around steel nail on the underneath of an insulator has the highest current density and temperature rise. As a result of strong partial evaporation, dry bands appear around the steel nail and cause discharges [23]. Meanwhile, in high voltage experiment, no continuous discharge can be observed by UV imager on the other parts of insulator. Therefore, the underneath of insulator is set as the objective of UV photography.

The type of UV imager used in this research is CoroCAM 504 (Council for Scientific and Industrial Research, Pretoria, South Africa). The UV imager was used in conjunction with a VDR-MC3 (Sony Group, Tokyo, Japan) video recorder. Output video format of the video recorder is vob. For the convenience of the subsequent process, vob-to-avi software was adopted to convert the video files from vob-to-avi format. Gain of the UV imager was set as 70%, threshold value was set as 40%, and photographic distance was 4 m. UV video shooting was synchronous with the shooting of IR image. Typical figures of UV images at 85% RH are shown in Figure 10. In images, white spots represent the discharge intensity.

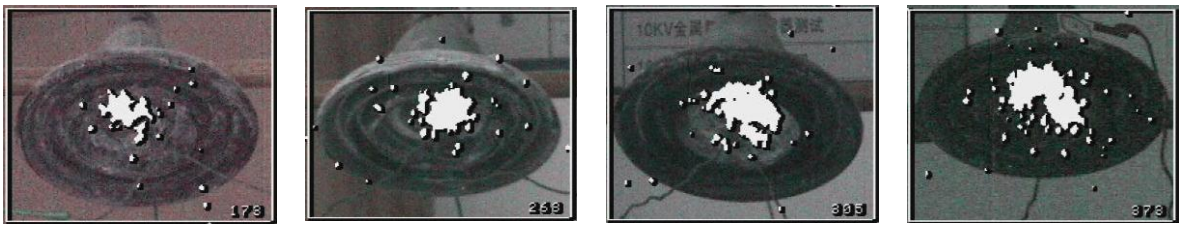

(**a**) (**b**) (**c**) (**d**)

Figure 10. Ultraviolet images of polluted insulators at 85% RH; (**a**) Insulator of I contamination grade; (**b**) Insulator of II contamination grade; (**c**) Insulator of III contamination grade; and (**d**) Insulator of IV contamination grade.

The UV videos were recorded at a rate of 25 frames per second. The size of UV image is 320 × 240. Electric discharges are displayed as white spots on UV images. Discharge intensity can be characterized by the number of white pixels (the area of white spots). In gray image, the gray values of white spots are close to 255. After analysis and comparison, gray value of 200 was selected as the threshold of white spot area calculation. Pixels with gray value larger than 200 were calculated as electric discharge white spots. And pixels with gray value smaller than 200 were considered background. According to this principle, pixel numbers of white spots were calculated for further processing.

Distribution curves of white spot pixels in 10 s (250 frames for each grade) at different RH are shown in Figure 11. Pixel numbers of insulators with high contamination grades are higher than that of insulators with low contamination grades. As is shown in Figure 11, UV images have abilities to characterize the differences of discharge intensities between each grade.

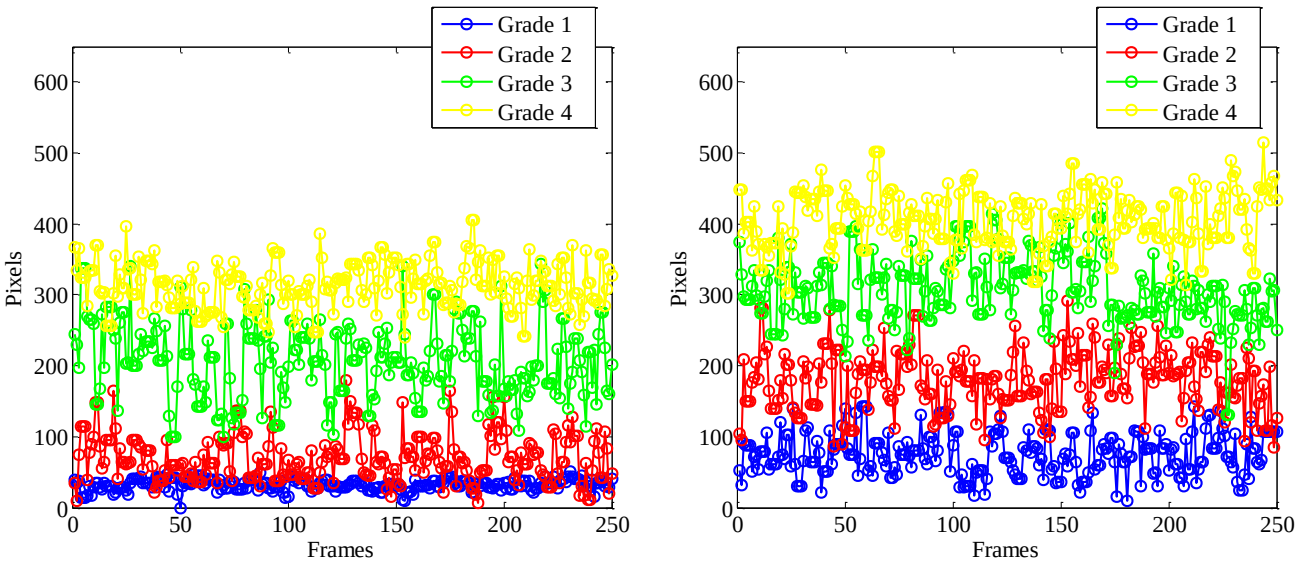

(**a**) (**b**)

Figure 11. *Cont.*

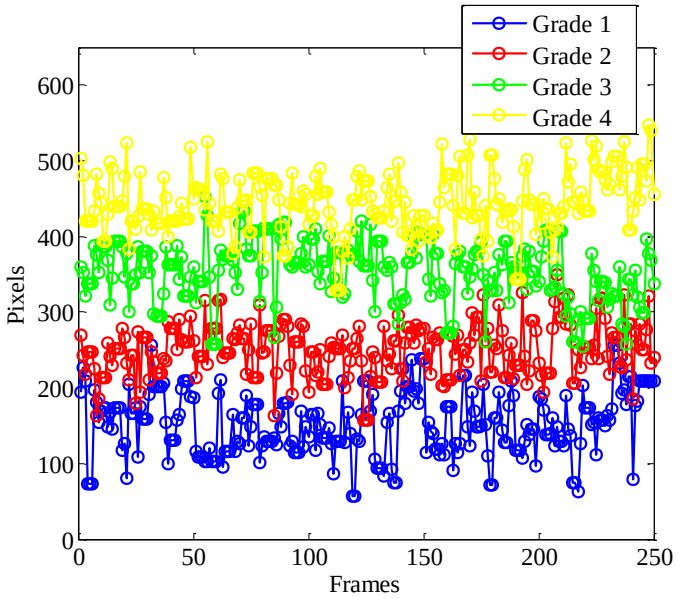

(**c**)

Figure 11. Distribution curves of white spot pixels in UV images. (**a**) RH = 80%; (**b**) RH = 85%; (**c**) RH = 90%.

2.4. Calculation of IR and UV Features

The calculation of IR and UV features is the basis of subsequent processing and classification. For each IR image, 11 statistics of relative temperature (difference between object temperature and ambient temperature) in insulator region were calculated as IR features. The statistics are listed as mean, median, maximum, minimum, mode, range, variance, skewness, kurtosis, energy and entropy. UV videos were divided into groups with an interval of 4 s. There were 100 images in each group. Number of white pixels in each image was calculated to characterize the discharge intensity. Mean, median, maximum, minimum, mode, range, variance, skewness, kurtosis, energy and entropy of the pixel numbers in each group were calculated as UV features. Formulas of some statistics are as follows:

Mean r_{aver}:

$$r_{aver} = \sum_i t(i)p_t\,(i) \tag{10}$$

Variance r_{var}:

$$r_{var} = \sum_i [t(i) - r_{aver}]^2\, p_t\,(i) \tag{11}$$

Skewness r_{skew}:

$$r_{skew} = \frac{\sum_i [t(i) - r_{aver}]^3\, p_t\,(i)}{\sqrt[3]{r_{var}}} \tag{12}$$

Kurtosis r_{kurt}:

$$r_{kurt} = \frac{\sum_i [t(i) - r_{aver}]^4 \, p_t(i)}{r_{var}{}^2} \tag{13}$$

Energy r_{ener}:

$$r_{ener} = \sum_i t(i)^2 p_t(i) \tag{14}$$

Entropy r_{entr}:

$$r_{entr} = \sum_i -p_t(i) \, lg(p_t(i)) \tag{15}$$

where $t(i)$ represents the sample value, $p_t(i)$ is the probability of $t(i)$, i is the serial number of sample value $t(i)$.

2.5. Feature Selection Based on Fisher Criterion

As mentioned above, feature sets of IR and UV images can be obtained after preprocessing and feature calculation. However, only a part of information is useful for the identification of contamination grades. Moreover, the irrelevant information degrades the recognition accuracy and increases the computing complexity. Therefore, selecting a subset of features containing the discriminative information is very important for the contamination grades recognition. In our research, Fisher criterion was applied to select powerful features from initial feature sets. Ratio of inter-class variance to intra-class variance is the evaluating indicator of Fisher criterion [24].

Supposing the number of samples in data set is n. The samples belong to different classes, which are given as $\omega_1, \omega_2, \ldots, \omega_C$, where C is the number of classes (in this paper, it is four). The number of samples in each class is given as n_i, i=1, 2, 3, 4. $S_B^{(k)}$ is the inter-class variance of feature k. And $S_\omega^{(k)}$ is the intra-class variance of feature k. k is the dimension (feature number) of sample x. Formulas of $S_B^{(k)}$ and $S_\omega^{(k)}$ are given as:

$$S_B^{(k)} = \sum_{i=1}^{C} \frac{n_i}{n} (m_i^{(k)} - m^{(k)})^2 \tag{16}$$

$$S_\omega^{(k)} = \frac{1}{n} \sum_{i=1}^{C} \sum_{x \in \omega_i} (x^{(k)} - m_i^{(k)})^2 \tag{17}$$

where $x^{(k)}$ is the value of feature k in sample x, $m_i^{(k)}$ is the mean value of feature k in class i, $m^{(k)}$ is the overall mean of feature k. Discriminant function of Fisher criterion is given as:

$$J_F(k) = \frac{S_B^{(k)}}{S_\omega^{(k)}} \tag{18}$$

J_F(k) is the criterion of feature k. Value of J_F represents the differential degree of the feature. Generally speaking, if the J_F of a feature is larger than two, this feature has sufficient capacity for differentiating.

2.6. Feature Fusion Based on Kernel Principal Component Analysis (KPCA)

The serial combination of two types of selected features is the ordinary feature level fusion method. However, high dimensionality and redundancy of the combined feature increase the computing time of classifier and decrease the accuracy of recognition. KPCA has strong capability of dimension reduction and redundancy elimination. Fused features with strong classification ability can be extracted from the combined features by the utilizing of KPCA [25]. Meanwhile, because of the dimension reduction, computational burdens of subsequent recognition can be eased significantly. On the basis of above analysis, KPCA was adopted to realize the fusion of IR and UV selected features in our research.

In KPCA, input data are transformed into a higher dimensional linear feature space by kernel function mapping. And then, principal component analysis (PCA) is adopted to process the mapping data in high-dimensional feature space and extract principal components, which can represent the characteristics of different contamination grades. Because of the capability of non-linear feature extraction, KPCA can extract the feature set which is more suitable in categorization than conventional PCA.

Supposing $x_k \in R^{M\times 1}$ is the original feature matrix, where k = 1, 2, 3, …, N, M is the dimension of feature set, N is the number of samples. Original feature space R is mapped onto high-dimensional feature space F by nonlinear mapping φ. Supposing the mapping data is zero-mean, the covariance matrix of mapping data is given as [26]:

$$C = \frac{1}{N}\sum_{n=1}^{N} \varphi(x_n)\varphi(x_n)^T \tag{19}$$

After the eigenvector analysis of C, we can derive that $Cv_i = \lambda_i v_i$. i is the number of eigenvalues and eigenvectors. It can be derived from Equation (19) that:

$$C = \frac{1}{N}\sum_{n=1}^{N} \varphi(x_n)[\varphi(x_n)\cdot v_i] = \lambda_i v_i \tag{20}$$

where

$$v_i = \sum_{n=1}^{N} \alpha_{in}\varphi(x_n) \tag{21}$$

After putting Equation (21) into Equation (20), a new expression of Equation (20) is given as:

$$\frac{1}{N}\sum_{n=1}^{N} \varphi(x_n)\varphi(x_n)^T \sum_{m=1}^{N} \alpha_{im}\,\varphi(x_m) = \lambda_i \sum_{n=1}^{N} \alpha_{in}\,\varphi(x_n) \tag{22}$$

Defining K as kernel matrix, where

$$K(x_n, x_m) = [\varphi(x_n)\cdot\varphi(x_m)] = \varphi(x_n)^T\varphi(x_m) \tag{23}$$

When both sides of Equation (22) are multiplied by $\varphi(x_l)^T$, it can be seen that:

$$\frac{1}{N}\sum_{n=1}^{N} K(x_l, x_n) \sum_{m=1}^{N} \alpha_{im}\,K(x_n, x_m) = \lambda_i \sum_{n=1}^{N} \alpha_{in}\,K(x_l, x_n) \tag{24}$$

Equation (24) can be expressed as $KK\alpha_i = \lambda_i NK\alpha_i$. The simplified formula is:

$$K\alpha_i = \lambda_i N\alpha_i \tag{25}$$

where α_i is a N-dimensional column vector composed by α_{ni}. Kernel principal component can be calculated as:

$$y_i(x) = \varphi(x)^T v_i = \sum_{n=1}^{N} \alpha_{in} K(x, x_n) \tag{26}$$

Above equations are derived under the hypothesis that the mapping data have the characteristic of zero-mean. Generally speaking, this hypothesis is untenable in practice. Therefore, the mapping data need to be centralized. In order to realize the centralization, K in Equation (25) is substituted by $\overline{K}$, where

$$\overline{K} = K - I_N K - K I_N + I_N K I_N \tag{27}$$

I_N is a $N \times N$ matrix with element of $1/N$. Inner product operation needs to be carried out in the process of extracting nonlinear principal component. In order to simplify the calculation, inner product operation is substituted by kernel function. Compared with other kernel functions, classifying quality of radial basis function (RBF) is the best. Formula of RBF is:

$$K(x, y) = \exp(-\frac{\|x - y\|^2}{2\sigma^2}) \tag{28}$$

where σ is the width parameter of RBF. Cumulative contribution ratio γ_k is the evaluation index of kernel principal component selection. Kernel principal component contribution ratio ρ_i and cumulative contribution ratio γ_k are given as [27]:

$$\rho_i = \lambda_i / \sum_{j=1}^{N} \lambda_j \ (i = 1, 2, 3, \ldots, N) \tag{29}$$

$$\gamma_k = \sum_{i=1}^{k} \rho_i \ (k = 1, 2, 3, \ldots, N) \tag{30}$$

k is the number of selected kernel principal components. N is the total number of kernel principal components, which equals to the number of analyzed samples. The importance of selected kernel principal components is reflected by ρ_i and γ_k. When γ_k is equal to or greater than 90%, the selected kernel principal components contain the main information of original data matrix and are suitable for subsequent classification.

2.7. PSO-BPNN Classifier

Constructing an effective classifier is of great importance in this study. Artificial neural network (ANN), which has a high degree of self-learning, self-organization and adaptive capacity, can be used in many problems, such as modeling, pattern recognition and prediction, *etc*. Back propagation neural network (BPNN) classifier was applied to the recognition of contamination grades in this paper. Neural network input includes the fused features and corresponding RH. Neural network output is contamination grade. Because BPNN is easy to fall into local optimum, the global optimal solution is difficult to be

guaranteed in training process. Meanwhile, problems, such as slow convergence speed and low accuracy, also restrict the application effect of BPNN. In order to overcome these disadvantages, particle swarm optimization (PSO) was used to optimize the training process of BPNN.

PSO is a kind of bionic optimization algorithm based on the imitation of bird foraging behavior. Every particle has three parameters: Position, velocity and fitness function. Position is a possible optimal solution for the optimization problem (in this study, the optimization problem is the adjustment of weights and thresholds of network neurons). Particle velocity (including direction and value) is dynamically adjusted towards local optimum and global optimum in light of experiences of the individual and the group. Fitness function value is calculated by objective function of optimization. In iteration, position and velocity of a particle are updated on the basis of individual extreme (a position with the minimum fitness value that a certain particle has ever experienced) and group extreme (position of a particle, which has the minimum fitness value in whole swarm). Individual extreme is the optimum position experienced by an individual particle. Group extreme is the global optimum position found by all particles. Positions and velocities are adjusted based on individual extreme and group extreme at each step of iteration. Meanwhile, individual extreme and group extreme are also updated according to the fitness function value. After certain steps of iteration, a particle with best fitness is taken as the optimal solution of optimization problem. Compared with other optimization algorithms, PSO has lower complexity and fewer parameters to regulate.

Supposing there are m particles in a swarm, position vector of particle i is $X_i = [x_{i1}, x_{i2}, \dots, x_{in}]$ (in this study, position vector is composed of weights and thresholds of neurons), velocity vector is $V_i = [v_{i1}, v_{i2}, \dots, v_{in}]$, n is the total number of optimized parameters. According to fitness function, fitness value of every position can be calculated. $P_i = [p_{i1}, p_{i2}, \dots, p_{in}]$ is defined as the individual extreme, $P_g = [p_{g1}, p_{g2}, \dots, p_{gn}]$ is defined as the group extreme of whole swarm. At each step of iteration, velocity and position of a particle are updated in accordance with Equations (31) and (32).

$$v_{ij}(t+1) = \omega v_{ij}(t) + c_1 r_1 \left[p_{ij}(t) - x_{ij}(t)\right] + c_2 r_2 \left[p_{gj}(t) - x_{ij}(t)\right] \quad (31)$$

$$x_{ij}(t+1) = x_{ij}(t) + v_{ij}(t+1) \quad (32)$$

where i is the particle number, j is the parameter number, c_1 and c_2 are learning factors, r_1 and r_2 are random numbers at the range of [0,1], ω is inertia weight. Inertia weight is dynamically adjusted as follows:

$$\omega = \omega_{max} - \frac{\omega_{max} - \omega_{min}}{t_{max}} \times t \quad (33)$$

where ω_{max} is initial inertia weight, ω_{min} is the inertia weight at the end of iterative process, t is the number of current iteration, t_{max} is the maximum number of iteration. Mean square error (MSE) of BPNN outputs is selected as the fitness function. Computational formula of MSE is:

$$E = \frac{1}{P} \sum_{\lambda=1}^{P} \sum_{k=1}^{s} (u_k^\lambda - y_k^\lambda)^2 \ (\lambda = 1,2,3, \dots, P) \quad (34)$$

where P is the number of training samples, s is the number of output neurons, u represents the actual output of BPNN, y represents the desired output of BPNN. The first part of Equation (31) represents influence of current velocity to next iteration; the second part represents the influence of individual

extreme (individual experience); the third part represents the influence of group extreme (group experience). In training process of PSO-BPNN, weights and thresholds of neurons are adjusted in accordance with PSO principle mentioned above.

3. Results and Discussion

3.1. Feature Calculation and Selection of IR Images

Forty IR images for each contamination grade at 80%, 85% and 90% RH were processed, respectively, in this section. After the extraction of insulator region using mathematical morphology improved Otsu algorithm, IR features mentioned in 2.4 were calculated. Then normalization was adopted to distribute the feature data in range of [0,1]. This processing ensures a uniform statistical distribution of each input datum for an artificial neural network (ANN) classifier. If the input data are not of the same order of magnitude, the convergence speed and identifying accuracy of the ANN may decrease [28]. The normalization formula is shown as:

$$\overline{r_i^{(k)}} = \frac{r_i^{(k)} - r_{min}^{(k)}}{r_{max}^{(k)} - r_{min}^{(k)}} \tag{35}$$

where $\overline{r_i^{(k)}}$ is the normalized value of a datum, $r_i^{(k)}$ is the original value of the datum, k = 1, 2, ..., 11 is feature number, i is sample number, $r_{min}^{(k)}$ and $r_{max}^{(k)}$ are the minimum and maximum values of feature k. After the normalization, Fisher criterions (J_F) of 11 sets of features at different RH are calculated and shown in Figure 12.

Value of J_F indicates the classifying quality of the feature. As mentioned in 2.5, a feature is suitable for classification if J_F is larger than two. Therefore, according to Figure 12, seven features, such as maximum, rang, variance, skewness, kurtosis, entropy and energy, were selected for further processing.

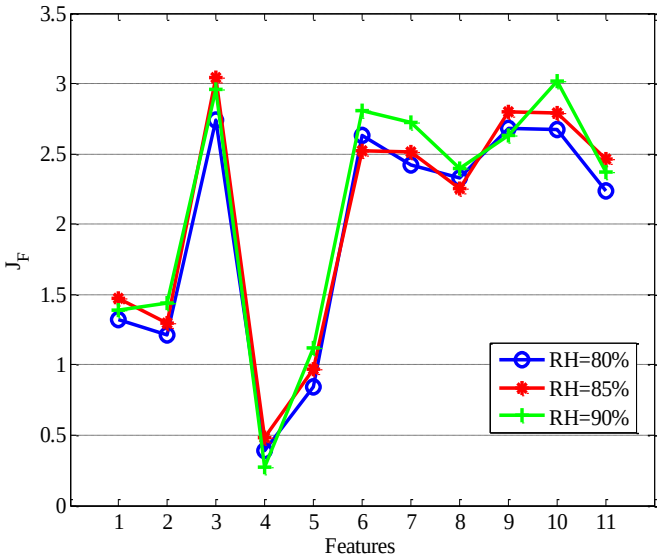

Figure 12. Fisher criterions of IR features. 1—Mean; 2—Median; 3—Maximum; 4—Minimum; 5—Mode; 6—Rang; 7—Variance; 8—Skewness; 9—Kurtosis; 10—Entropy; 11—Energy.

3.2. Feature Calculation and Selection of UV Images

After the preprocessing of UV videos, 40 groups of UV images for each contamination grade at 80%, 85% and 90% RH were obtained, respectively. UV features mentioned in 2.4 were calculated and normalized. The normalization formula is shown in Equation (35). Fisher criterions (J_F) of 11 sets of features at different RH were calculated and shown in Figure 13. Six features whose Fisher criterions were larger than two were selected for further processing, including mean, median, maximum, variance, skewness and energy.

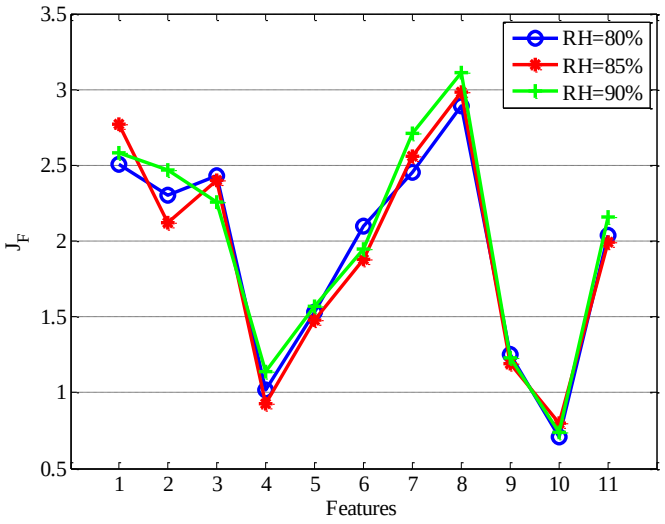

Figure 13. Fisher criterions of UV features. 1—Mean; 2—Median; 3—Maximum; 4—Minimum; 5—Mode; 6—Rang; 7—Variance; 8—Skewness; 9—Kurtosis; 10—Entropy; 11—Energy.

3.3. Contamination Grades Recognition Based on Feature Fusion

After seven IR features and six UV features had passed the feature selection, KPCA was applied to process the combination of IR and UV selected features and extract fused features. Kernel principal components number and RBF width are two important parameters of KPCA. Values of these two parameters directly affect the result of feature level fusion. Cumulative contribution ratios of the first three kernel principal components are shown in Figure 14. The RBF width parameter (σ) ranged from 0.1 to 10 at the interval of 0.1. As is shown in Figure 14, cumulative contribution ratios of the first three kernel principal components are larger than 90% at every relative humidity. As mentioned in Section 4, that means they have enough ability to recognize the contamination grades of insulators. Therefore, the first three kernel principal components were selected as the three-dimensional fused features for further classification.

On the whole, for the first three kernel principal components at different RH, distribution curves of cumulative contribution ratios become steady when σ reaches the value of 5. That means even the value of σ continues to increase, the classification ability of the corresponding feature will not enhance significantly. Hence the RBF parameters σ were set as 5 at every RH uniformly. Taking 40 samples of each grade, for example, distributions of three-dimensional fused features at 80%, 85% and 90% RH are shown in Figure 15.

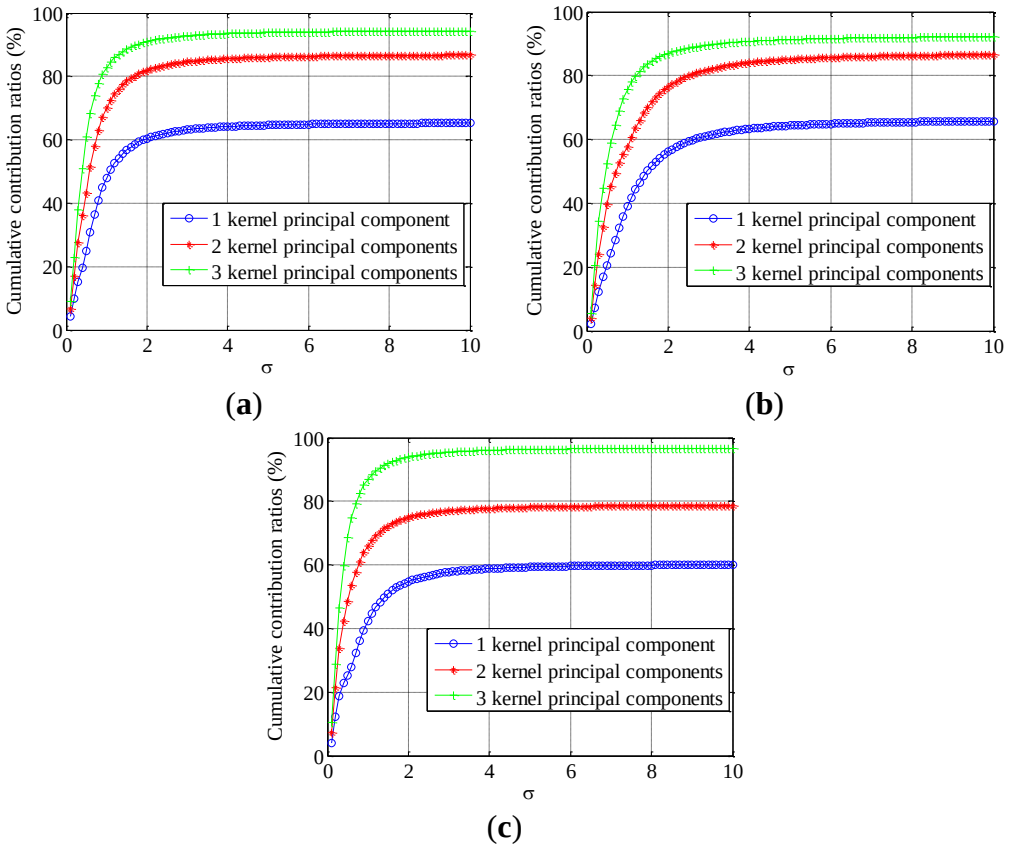

Figure 14. Cumulative contribution ratios of kernel principal components. (**a**) RH = 80%; (**b**) RH = 85%; (**c**) RH = 90%.

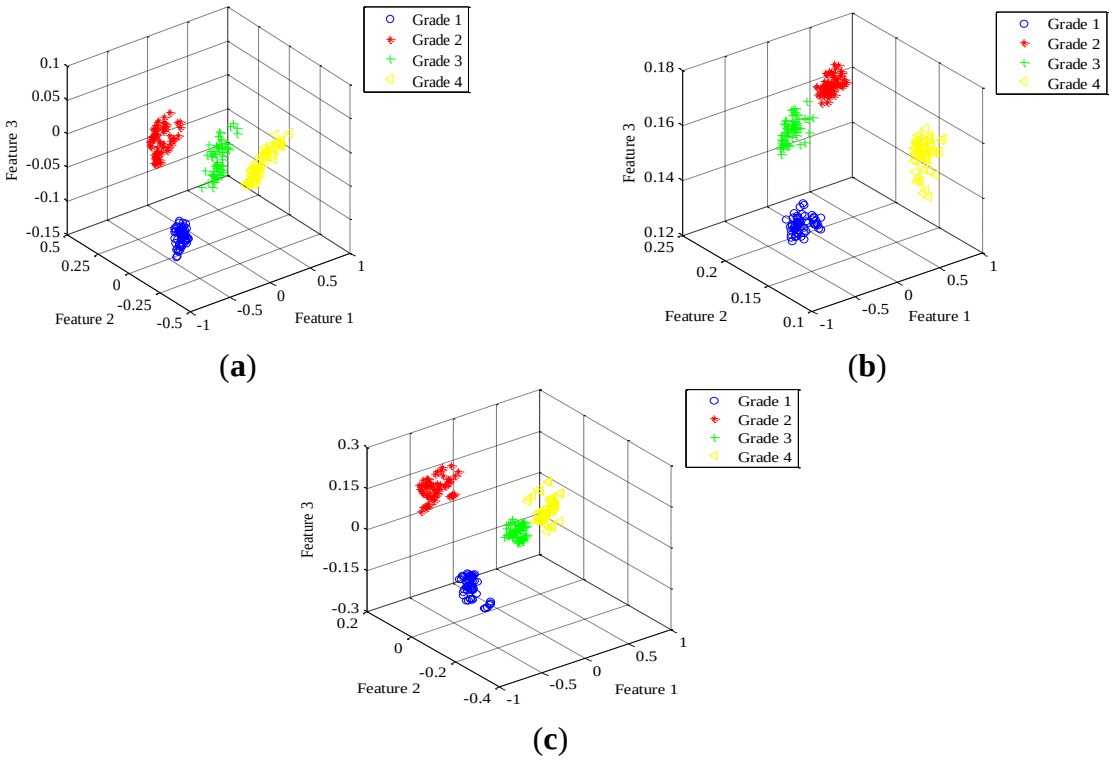

Figure 15. Distributions of three-dimensional fused features. (**a**) RH = 80%; (**b**) RH = 85%; (**c**) RH = 90%.

As is shown in Figure 15, the three-dimensional fused features have obvious clustering characteristics at every RH. As the differences in both IR and UV features are fully utilized by the KPCA procedure, distributions of four clusters of samples are different significantly.

After feature level fusion of IR and UV information, a PSO-BPNN classifier was constructed and trained for the contamination grades identification. Inputs of the neural network were three-dimensional fused feature set and corresponding RH. Outputs of the neural network were contamination grades. Number of neurons in input layer was four. Hidden layer neuron number was six. Output layer neuron number, which was equivalent to contamination grades, was four. In PSO algorithm, population size is 100, maximum iteration number is 100, learning factors c_1 and c_2 are defined as 2, particle dimension (number of optimized parameters) is 58. For a particle with size of 1×58, elements from 1 to 24 are connection weights between input layer neurons and hidden layer neurons; elements from 25 to 48 are connection weights between hidden layer neurons and output layer neurons; elements from 49 to 54 are thresholds of hidden layer neurons; Elements from 55 to 58 are thresholds of output layer neurons. Two hundred eighty training samples (70 for each grade) were utilized to train the PSO-BPNN. Weights and thresholds are optimized by PSO algorithm. Structure of the PSO-BPNN classifier is shown in Figure 16.

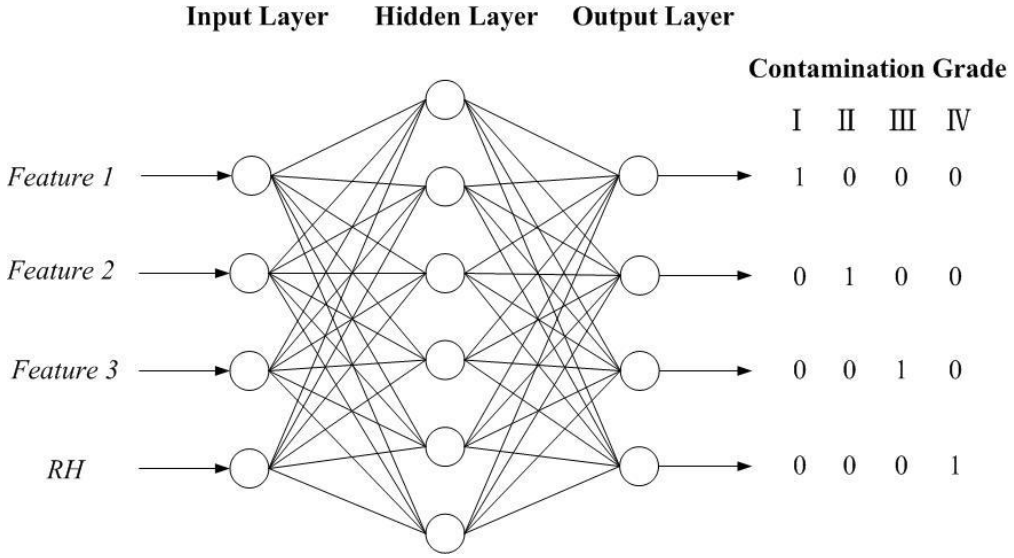

Figure 16. Structure of PSO-BPNN.

Four pieces of artificially polluted insulators with four different contamination grades (ESDD were 0.04, 0.08, 0.2 and 0.3 mg/cm^2 separately) were taken as the test group. One hundred twenty testing samples (30 for each grade) were selected to test the classifying effect. In order to validate the effect of feature level fusion, KPCA was used to extract three-dimensional feature sets from IR and UV selected features, respectively. After similar analyses as shown in Figure 14, RBF width parameters σ of KPCA for IR and UV features were set as 5. PSO-BPNN classifiers with same structure as Figure 16 were designed and trained. Results of contamination grades recognition using IR, UV and fused features are shown in Table 1.

Table 1. Results of contamination grades recognition.

Contamination grades	Actual number	Numbers of correctly recognized samples		
		IR features	UV features	Fused features
I	30	24	22	29
II	30	23	23	28
III	30	26	23	29
IV	30	25	23	30
Accuracy Rate	–	81.67%	75.83%	96.67%

The accuracy rate of recognition was defined as:

$$P_i = \frac{N_i}{N_{sum}} \times 100\% \tag{36}$$

where N_i is the number of correctly recognized samples, N_{sum} is the total number of samples, i = 1, 2, 3 represent IR, UV and fused features, respectively.

As is shown in Table 1, accuracy rate of contamination grades recognition using IR features is 81.67% and for UV features, the accuracy rate is 75.83%. In contrast, the accuracy of recognition using fused features is 96.67%. One can see that, compared with using IR or UV features solely, the fused feature is more satisfactory for a high precision measurement. The feature level fusion of IR and UV image information has the capability to realize the high accuracy recognition of insulator contamination grades. At present, inspections of power equipment using IR and UV cameras are usually arranged at windless night to avoid disturbance from sunlight and other environmental disturbance. Meanwhile, when relative humidity is less than 75%, the leakage current value is relatively small; temperature rise and discharge are not obvious. Therefore, the proposed technique is suggested to be utilized on windless nights (RH is relatively high at night). With the development of study, research can be carried out at more various relative humidity, such as 83% and 87% so as to further improve the accuracy and applicability.

4. Conclusions

This paper has proved that it was feasible to accurately recognize insulator contamination grades using fused information from both IR and UV images. It was demonstrated that feature level fusion significantly improves the recognition performance over a single information source. Fisher criterion was applied to select powerful features from the original feature sets of IR and UV images. And then, KPCA was adopted to carry out feature level fusion and obtain fused features. After that, a PSO-BPNN classifier was introduced to realize the accurate identification of contamination grades. Experimental results show that KPCA is an effective feature level fusion method, which has a strong ability of multi-source information processing. Compared with recognition using IR or UV features separately, the fused features can take advantage of information from both IR and UV images and characterize the contamination state comprehensively. As the fused features contain more effective information than any single type of image feature, the precision of contamination grades recognition is improved by information fusion significantly.

Acknowledgments

This work was supported by the National Natural Science Foundation of China under Grant No. 51177109 and State Key Laboratory of Electrical Insulation and Power Equipment under Grant No. EIPE14211.

Author Contributions

All the authors contributed equally to this work.

Conflicts of Interest

The authors declare no conflict of interest.

References

1. Working Group 33.13. Polluted insulators: A review of current knowledge. CIGRE Task Force 33.04.01 Report. *Brochure* **2000**, *158*, 5–6.
2. International Electrotechnical Commission (IEC). *Selection and Dimensioning of High-Voltage Insulators Intended for Use in Polluted Conditions-Part 2: Ceramic and Glass Insulators for A.C. Systems*; Technical Report IEC 60815-2; IEC: Geneva, Switzerland, 2008.
3. Slama, M.E.I.-A.; Beroual, A.; Hadi, H. Analytical computation of discharge characteristic constants and critical parameters of flashover of polluted insulators. *IEEE Trans. Dielectr. Electr. Insul.* **2010**, *17*, 1764–1771.
4. Li, J.Y.; Sun, C.X.; Sebo, S.A. Humidity and contamination severity impact on the leakage currents of porcelain insulators. *IET Gner. Transm. Distrib.* **2011**, *5*, 19–28.
5. Reddy, B.S.; Nagabhushana, G.R. Study of temperature distribution along an artificially polluted insulator string. *Plasma Sci. Technol.* **2003**, *5*, 1715–1720.
6. He, H.Y.; Yao, J.G.; Jiang, Z.L.; Li, W.W. Contamination grades recognition of insulators under different humidity using infrared image features and RBPNN. *Proc. CSEE* **2006**, *26*, 117–123.
7. Li, Z.S.; Li, W.L.; Yao, J.G.; Yang, Y.J. On-site detection of pollution level of insulators based on infrared-thermal-image processing. *Proc. CSEE* **2010**, *30*, 132–138.
8. Da Costa, E.G.; Ferreira, T.V.; Neri, M.G.G.; Queiroz, I.B.; Germano, A.D. Characterization of polymeric insulators using thermal and UV imaging under laboratory conditions. *IEEE Trans. Dielectr. Electr. Insul.* **2009**, *16*, 985–992.
9. Li, H.M.; Wang, S.H.; Lv, F.C.; Liu, Y.P.; Chen, L.; Wei, J.X. Contamination condition evaluation of insulators based on discharge ultraviolet imaging parameters. *Trans. China Electrotech. Soc.* **2010**, *25*, 22–29.
10. Krystian, L.C.; Wallace, L.V.; Jacobus, P.H. Leakage current on porcelain and silicone insulators under sea or light industrial pollution. *IEEE Trans. Power Del.* **2011**, *26*, 2051–2252.
11. Krystian, L.C. Leakage currents on naturally contaminated porcelain and silicone insulators. *IEEE Trans. Power Del.* **2010**, *25*, 904–910.
12. Isaias, R.; Ramiro, H.; Gerardo, M. Measurement of leakage current for monitoring the performance of outdoor insulators in polluted environments. *IEEE Electr. Insul. Mag.* **2012**, *28*, 29–34.

13. Pylarinos, D.; Siderakis, K.; Pyrgioti, E. Measuring and analyzing leakage current for outdoor insulators and specimens. *Rev. Adv. Mater. Sci.* **2011**, *29*, 31–53.
14. Li, J.Y.; Sun, C.X.; Sima, W.X.; Yang, Q.; Hu, J.L. Contamination level prediction of insulators based on the characteristics of leakage current. *IEEE Trans. Power Del.* **2010**, *25*, 417–424.
15. Chen, W.G.; Wang, W.W.; Xia, Q.; Luo, B.; Li, L.C. Insulator contamination forecasting based on fractal analysis of leakage current. *Energies* **2012**, *5*, 2594–2607.
16. Pylarinos, D.; Theofilatos, K.; Siderakis, K.; Thalassinakis, E.; Vitellas, I.; Alexandridis, A.T.; Pyrgioti, E. Investigation and classification of field leakage current waveforms. *IEEE Trans. Dielectr. Electr. Insul.* **2012**, *19*, 2111–2118.
17. Li, H.L.; Wen, X.S. Statistical fingerprint analysis for contaminated insulator acoustic emission signals. *High Volt. Eng.* **2010**, *36*, 2705–2710.
18. Gubanski, S.M.; Dernfalk, A.; Andersson, J.; Hillborg, H. Diagnostic methods for outdoor polymeric insulators. *IEEE Trans. Dielectr. Electr. Insul.* **2007**, *14*, 1065–1080.
19. Han, C.Z.; Zhu, H.Y.; Duan, Z.S. *Multisource Information Fusion*; Tsinghua University Press: Beijing, China, 2010; pp. 2–4.
20. Zakaria, A.; Shakaff, A.Y.M.; Masnan, M.J.; Saad, F.S.A.; Adom, A.H.; Ahmad, M.N.; Jaafar, M.N.; Abaullah, A.H.; Kamarudin, L.M. Improved maturity and ripeness classifications of *Magnifera indica* cv. Harumanis mangoes through sensor fusion of an electronic nose and acoustic sensor. *Sensors* **2012**, *12*, 6023–6048.
21. Liu, D.; Sun, D.M.; Qiu, Z.D. Feature level fusion based on speaker verification via relation measurement fusion framework. *Acta Auto. Sin.* **2011**, *37*, 1503–1513.
22. Zhu, X.F.; Ma, C.W.; Liu, B. Aircraft recognition scheme based on feature fusion and support vector machine. *J. Optoelectron. Laser* **2011**, *22*, 1710–1713.
23. Mei, H.W.; Wang, L.M.; Guan, Z.C. Influence of sugar as a contaminant on outdoor insulation characteristics of insulators in a substation. *IEEE Trans. Dielectr. Electr. Insul.* **2012**, *19*, 1318–1324.
24. Yang, J.; Yang, J.Y.; Ye, H. Theory of Fisher linear discriminant analysis and its application. *Acta Auto. Sin.* **2003**, *29*, 481–493.
25. Li, X.J.; Li, P.; Jiang, L.L.; Cao, Y.X. Fault diagnosis method of asynchronous motor based on heterogeneous information feature fusion. *Chin. J. Sci. Instrum.* **2013**, *34*, 228–233.
26. Li, N.; Zhang, Y.Y.; Li, Y.J. Fault identification algorithm by redundancy supervision based on KPCA method. *J. Syst. Simul.* **2011**, *23*, 2079–2088.
27. Li, W.H.; Liao, G.L.; Shi, T.L. Kernel principal component analysis and its application in gear fault diagnosis. *Chin. J. Mech. Eng.* **2003**, *39*, 65–70.
28. Bashir, N.; Ahmad, H. Odd harmonics and third to fifthharmonics ratios of leakage currents as diagnostic tools to study the ageing of glass insulators. *IEEE Trans. Dielectr. Electr. Insul.* **2010**, *17*, 819–832.